Eur. Phys. J. E (2006)
DOI 10.1140/epje/i2005-10057-y

THE EUROPEAN PHYSICAL JOURNAL E

Spinodal wrinkling in thin-film poly(ethylene oxide)/polystyrene bilayers

J.S. Sharp[1,a], D. Vader[2,3], J.A. Forrest[2,b], M.I. Smith[1], M. Khomenko[2], and K. Dalnoki-Veress[4]

[1] School of Physics and Astronomy, University of Nottingham, Nottingham, NG7 2RD, UK
[2] Department of Physics and Guelph-Waterloo Physics Institute, University of Waterloo, Waterloo, Ontario, N2L 3G1, Canada
[3] Division of Engineering and Applied Sciences, Harvard University, Cambridge, MA 02138, USA
[4] Department of Physics and Astronomy, McMaster University, Hamilton, Ontario, L8S 4M1, Canada

Received 8 November 2005 /
Published online: 13 April 2006 –

Abstract. Optical microscopy and atomic force microscopy were used to study a novel roughness-induced wrinkling instability in thin-film bilayers of poly(ethylene oxide) (PEO) and polystyrene (PS). The observed wrinkling morphology is manifested as a periodic undulation at the surface of the samples and occurs when the bilayers are heated above the melting temperature of the semi crystalline PEO (T_m = 63 °C) layer. During the wrinkling of the glassy PS capping layers the system selects a characteristic wavelength that has the largest amplitude growth rate. This initial wavelength is shown to increase monotonically with increasing thickness of the PEO layer. We also show that for a given PEO film thickness, the wavelength can be varied independently by changing the thickness of the PS capping layers. A model based upon a simple linear stability analysis was developed to analyse the data collected for the PS and PEO film thickness dependences of the fastest growing wavelength in the system. The predictions of this theory are that the strain induced in the PS layer caused by changes in the area of the PEO/PS interface during the melting of the PEO are sufficient to drive the wrinkling instability. A consideration of the mechanical response of the PEO and PS layers to the deformations caused by wrinkling then allows us to use this simple theory to predict the fastest growing wavelength in the system.

PACS. 68.55.-a Thin film structure and morphology – 61.41.+e Polymers, elastomers, and plastics – 68.35.Ct Interface structure and roughness – 68.35.Ja Surface and interface dynamics and vibrations

Introduction

Pattern formation processes are becoming increasingly attractive as methods for producing nano and microscale structured materials and surfaces. For example, the use of macromolecular self-assembly to form regular and predetermined patterns on a micron or sub-micron length scale is a focus for intense research. Perhaps the area of greatest recent emphasis is on trying to manipulate the mesostructures formed in block copolymer melts, for instance by exploiting the different interactions between the two polymer species and a substrate [1]. Other techniques have also been used to control the length scale and anisotropy of phase-separating polymer blend systems, or dewetting polymer films [2]. A common theme in many of these studies is to produce a physical or chemical template on the substrate that can be used to direct the controlled self-assembly of the physical system of interest. A disadvantage of this approach is that it requires manipulation of material on small length scales and the preformation of an existing pattern or template before the desired structures can be obtained. A more desirable approach is to obtain microscopic structures by using competing physical processes that favour structure formation on different lengthscales. Examples of these so-called kinetic lengthscale selection processes include the spinodal decomposition of binary mixtures and spinodal dewetting in ultrathin polymer films [2]. Another example of this type of process is the so-called "dispersion driven morphology" studied by Dalnoki-Veress *et al.* [3]. In the most simple case of a freely standing rubbery film sandwiched between rigid capping layers, the dispersion forces between the two capping layers drive the interfaces together. Since the fluid layer is incompressible, the competition between the bending energy of the capping layer and the flow of the liquid leads to a definite length scale in the resulting morphology. The linear stability analysis theory derived in the work by Dalnoki-Veress *et al.* is applicable to almost any driving force, and more recently Schäffer *et al.* [4] used a similar

[a] e-mail: james.sharp@nottingham.ac.uk
[b] e-mail: jforrest@uwaterloo.ca

theoretical approach to describe how electric fields can be used to drive a wrinkling instability in air gap capacitors containing ultrathin polymer films.

Other physical phenomena have also been shown to lead to controllable and highly oriented morphologies. One specific example is the work by Bowden *et al.* [5]. In this case a thin film of poly(dimethyl siloxane) was crosslinked and capped with a rigid metallic film. During the deposition (or preparation) of the capping layer, the system was at elevated temperatures. The differences in the thermal expansion coefficients of the metal and polymer layers resulted in a differential amount of contraction when these bilayers were subsequently cooled. This caused the bilayer structures to buckle. Similar morphologies have also been observed in mechanically loaded bilayer samples. The differential strains that drive the formation of these morphologies often arise as a result of differences in the Young's moduli of the bilayer materials being used [6]. Thin-film buckling has also been observed as the result of the differential swelling response of polymer films supported on inorganic substrates [7,8].

The stresses that evolve in these types of system are clearly large enough to cause the layers in the system to buckle. However, rather than buckling with the lowest energy mode in such a way as to minimise the amount of bending stress in the buckled films, the presence of the attachment of the different layers can result in the system wrinkling on short length scales. In the case of the wrinkling of elastic plates on the surface of viscous [9, 10] and viscoelastic [11] substrates, the short-wavelength wrinkling occurs because of kinetic constraints that are imposed on the system because of the need to transport material in the underlying layer to accommodate the wrinkling of the film attached to its surface. In the case of an elastic film that is bonded to an elastic substrate, adhesion plays a crucial role. The structures that form in these elastic-elastic bilayer systems depend upon whether or not the elastic energy stored in the films is sufficient to overcome the adhesive interactions between the layers. In the case when adhesion energies are large compared to the elastic energy, periodic one-dimensional wrinkles are usually formed at the surface of the bilayer [6] and when the adhesive energies are small, circular blisters are usually observed [7].

In all of the above cases, the buckling/wrinkling instabilities result in the production of structures at the surface of the bilayer that have a well-defined size or wavelength. The size of the structures typically depends upon the mechanical properties and/or the thickness of the various layers. The characteristic lateral size of the structures that form in these sytems is typically on the order of a few microns to a few tens of microns in size.

In this manuscript we investigate a wrinkling morphology that is observed during the heating of thin-film bilayers of poly(ethylene oxide) (PEO) and polystyrene (PS) supported on single-crystal silicon substrates. We show that the wrinkling instability is driven by changes in the PEO/PS interfacial area that occur during the melting of the underlying PEO layer. The change in the area of this interface results in an in-plane compressive stress being generated in the glassy PS films that are used to cap the PEO layers. We analyse the data for the wrinkling wavelength with the fastest growing amplitude using a simple linear stability analysis that considers the balance between the compressive and bending stresses in the wrinkling PS films as well as the normal pressure exerted on the PS films due to the viscoelastic response of the confined molten PEO layer. We show that this simple theory can be used to gain good agreement with experiment if the initial strain in the PS films and the bulk mechanical properties of the PS and PEO layers are known.

Experimental

Thin films of poly(ethylene oxide) (PEO, M_w = 11300 g/mol, $M_w/M_n = 1.08$, Polymer Source Inc.) were spin cast onto 1 cm × 1 cm single-crystal Si (100) wafers (Compart Technology) from solutions in chloroform using a spin speed of 3000 rpm. The thickness of the PEO films was controlled by varying the concentration of the solutions. PEO film thicknesses (h) in the range 65 nm to 533 nm were produced using this method. All the PEO films studied were heated to 70 °C on a hotplate for approximately 30 seconds (melting temperature, T_m of PEO = 63 °C). This was done to remove solvent and to relax any residual stresses in the PEO films that were introduced during spin coating. The thickness of the PEO films was determined at 70 °C using ellipsometry. The ellipsometry measurements yielded a best fit to the data when the value used for the refractive index of the PEO was $n_{PEO} = 1.462 \pm 0.002$. This value is consistent with literature values obtained for amorphous PEO [12]. The refractive index was fixed at this value and the thickness of the PEO films was determined by fitting the ellipsometric angles (P and A) obtained for each sample to the uniform thin slab model described by Azzam and Bashara [13] using a simplex algorithm. The only parameter in this fitting procedure was the thickness of the PEO film. Once the P and A values had been determined, the PEO films were quenched to room temperature and allowed to crystallise. The roughness of the spin cast PEO films was then measured using an Asylum Research MFP-3D atomic force microscope operating in intermittent contact mode. Measurements of the surfaces were taken over a number of scan sizes in the range 10 μm × 10 μm to 90 μm × 90 μm. In all cases both the total surface area and projected surface area of the samples were determined.

Polystyrene (PS) capping layers were prepared by spin coating solutions of PS (M_w = 654000 g/mol, M_w/M_n = 1.09, Polymer Source) on to clean glass slides from solutions in toluene. All the films were prepared using a spin speed of 3000 rpm and the PS film thickness was controlled by varying the concentration of the solutions. The unannealed PS films were then transferred on to the surface of deionised water before being picked up on a metal support using a method described elsewhere [14]. The support used contained a circular hole in it that was approximately 15 mm in diameter so that it was slightly larger

than the size of the Si wafers used as substrates for the PEO films. The PS films were picked up on this support, such that they covered the area with the hole but were supported at the edges. The resulting free standing films often contained wrinkles as a result of this water transfer technique. To remove these wrinkles all the PS films were placed over a hot plate at $\sim 100\,^{\circ}\mathrm{C}$ ($T_g(\mathrm{PS}) = 97\,^{\circ}\mathrm{C}$) and observed until all the defects had been removed. Care was taken at this point to ensure that the thin PS films did not form holes due to rupturing under the action of dispersion forces between the two film surfaces. PEO/PS bilayers were then prepared by carefully lowering the PS-covered metal support over the PEO-coated Si wafers. At the point where the PS film initially touched the semicrystalline PEO layer, surface forces acted to pull the remaining parts of the films into intimate contact and the PS films were found to faithfully follow the contours of the PEO surfaces. This procedure produced bilayer films with no observable defects or cracks. The samples were prepared in this way so that the thickness of the PEO and PS layers could be accurately controlled and also to minimise the width of the PEO/PS interface. Although these polymers are highly immiscible, the procedure of spin coating the polymers from mutually exclusive solvents may still result in significant swelling of the polymer layers and could result in significantly larger interfacial widths. The thickness of the PS capping layers was determined using parts of the same PS films that were used to produce the bilayer samples. This was done by transferring them separately from the deionised water surface on to a holder, where they were annealed above a hot plate at $\sim 100\,^{\circ}\mathrm{C}$ and transferred on to a clean Si wafer. Ellipsometry was then used to determine the thickness of the PS films using the same procedure outlined for the PEO films above. The refractive index of the polystyrene was determined to be $n = 1.595 \pm 0.001$ and was found to be consistent with literature values [12]. The range of PS film thicknesses (L) used was determined to be between 45 nm and 406 nm.

A series of bilayer films were produced by using different combinations of the PEO and PS film thicknesses. Atomic force microscopy (AFM) measurements were then performed on all of the bilayer samples to determine both the total area (A_{total}) of the samples and the projected area (A_{scan}) using the same scan parameters that were used for the PEO films described above. These AFM measurements showed that all the bilayers produced in this way had similar surface areas. These measurements were used to determine the areal strain introduced into the PS capping layers during the melting of the PEO layer, such that $\epsilon_{area} = \frac{A_{total}}{A_{scan}} - 1$. This result was then used to calculate the linear strain in the PS films using the expression $\epsilon_{lin} \approx \epsilon_{area}/2$. A range of values of $\epsilon_{lin} = (0.50 \pm 0.05) \times 10^{-3}$ was determined for all the samples studied.

The PEO/PS bilayers were then transferred to a Linkam THMS 600 hot stage and heated to 70 °C using a heating rate of 90 °C per minute. During heating, the samples were observed with an Olympus BX51 optical microscope using bright field illumination. The same level of illumination was used to view all of the bilayer samples studied and optical micrographs of the samples were collected using an Olympus DP70 camera that was connected to the microscope and a PC equipped with Image Pro Plus image analysis software (Media Cybernetics). At a temperature of $\simeq 65\,^{\circ}\mathrm{C}$ the underlying PEO layers were observed to melt and the surface structure

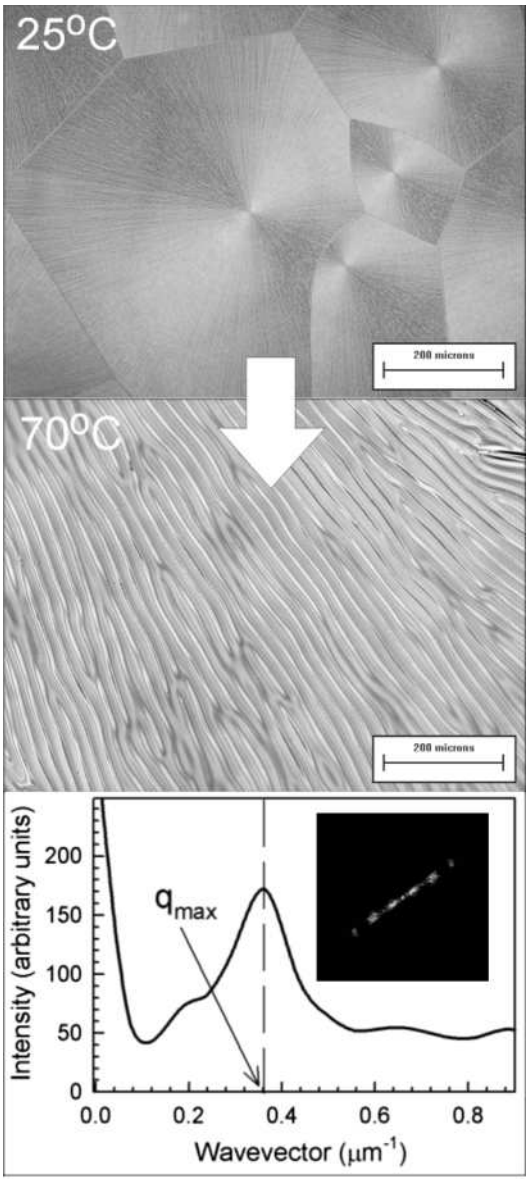

Fig. 1. Optical micrographs of a PEO/PS bilayer before and after heating to 70 °C. The top panel is an image of a 533±6 nm thick PEO film capped with a 143 ± 5 nm thick PS film taken at 25 °C and prior to heating. The bottom image is of the same sample taken immediately after heating to 70 °C. The characteristic lengthscale of the corrugations observed in this image is $\sim 17\,\mu$m. The bottom panel shows a line profile of the radial intensity distribution that was taken from the Fourier transform (FT) of the image (see inset) of the morphology shown in the middle panel. This line profile was taken along a line passing through the centre of the FT and the first peak.

changed from something similar to that of a semicrystalline PEO film to a structure that consisted of a series of periodic one-dimensional corrugations. Figure 1 shows an example of optical micrographs of a PEO/PS bilayer (PEO thickness = 533 ± 6 nm, PS thickness = 143 ± 5 nm) taken before and immediately (~ 1 second) after the PEO layer melted. The resulting images were saved and analyzed using the ImageProPlus software. A fast Fourier transform (FFT) of the images was then used to determine the image intensity distribution as a function of the wave vector, q. This distribution was determined along a line passing through the centre of the FFT and the first peak maximum. The dominant wave vector, q_{max} was then extracted from the position of the first peak (see bottom panel of Fig. 1) and the characteristic wavelength, λ, calculated using the expression $\lambda = 2\pi/q_{max}$. Values of λ determined in this way were found to agree with average values obtained directly from the real space image. Atomic force microscopy was then used to image the corrugated structures at room temperature, after the PEO layers had been isothermally recrystallised at a temperature of 50 °C. In each case the total and projected area of the samples was determined. Figure 2 shows examples of AFM images of an uncapped PEO surface and the surface of a PEO/PS bilayer that were taken before and after heating to 70 °C.

A key concern with these experiments is that the PS films may not be fully annealed by placing them over the hotplate and that residual stresses and/or solvent introduced during spin coating of the PS films may still have been present when the bilayer samples were prepared. If these stresses were still present, then they would be expected to modify the strains experienced by the PS capping layers and this would affect the observed wavelength of the wrinkling morphology (see below). To ensure that this was not the case and that residual stresses were not present in the PS films, we produced a series of bilayer films using PS capping layers that had been annealed at 130 °C under vacuum for 8 hours. The annealing of these samples was performed while the PS films were still supported on the glass substrates. The films were then cut and floated on to the surface of deionised water, before being picked up and placed on top of the PEO films using the water transfer procedure described above. The bilayer samples produced using the "substrate annealed" PS films displayed exactly the same wrinkling behaviour as the samples that were annealed over the hotplate as free standing membranes. The initial wrinkling wavelengths were measured to be the same within error for both sets of samples studied.

In addition to the samples described above, a third set of PEO/PS bilayers was prepared using the same method, but this time the PEO films were held at a temperature of 70 °C during the formation of the bilayers. Under these conditions, the PEO was in the molten state when the bilayer samples were prepared. These samples did not display the wrinkling morphology described above. This provides support to the idea that it is the melting of the PEO and the change in the PEO/PS interfacial area that drives the formation of the morphology. These observations also rule out the possibility that dispersion forces are responsible for driving the wrinkling instability, as these effects would also be present in bilayer samples that were prepared when the PEO was in the molten state.

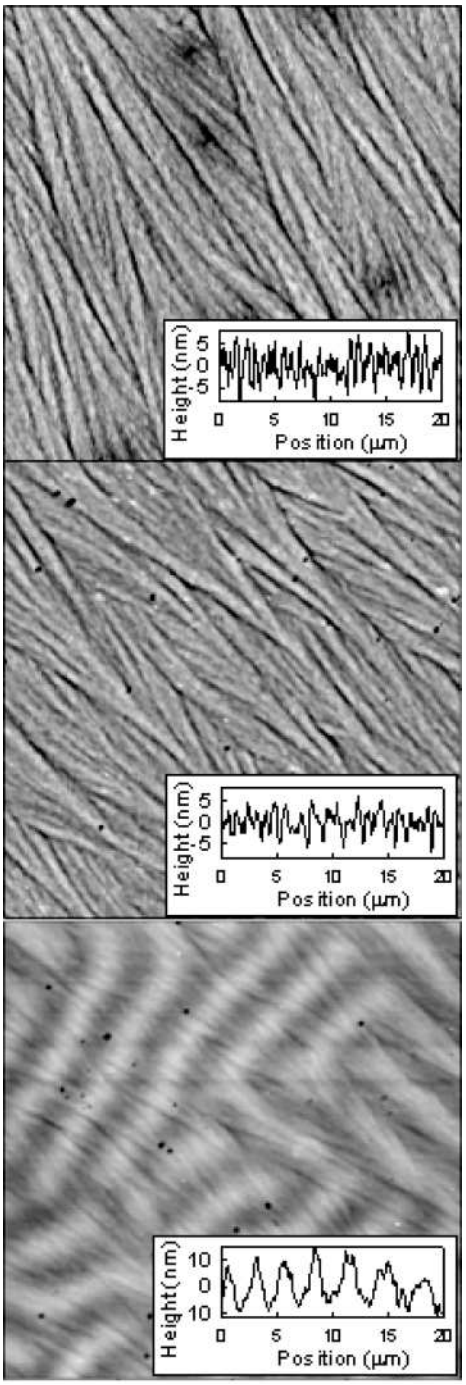

Fig. 2. Atomic force microcope images of a 65 ± 3 nm thick spin cast PEO film (top panel) and the same PEO film capped with a 44 ± 4 nm thick PS film (middle panel). Both of these images were taken at 25 °C. The bottom panel shows the same PEO/PS bilayer sample following heating to 70 °C and a rapid quench to 50 °C. All images were taken using a scan area of $20\,\mu\text{m} \times 20\,\mu\text{m}$. The insets show a typical distribution of heights taken along a single line scan at each stage of the sample preparation procedure.

The frequency-dependent rheological properties of bulk samples of PEO having a similar molecular weight ($M_w = 10000\,\mathrm{g/mol}$, Sigma) were also determined using a TA Instruments Rheometrics AHRES rheometer in the cone and plate geometry using a constant strain of 1%. A sample of the PEO was prepared by depositing the polymer on to the heated rheometer plate. The samples were then equilibrated at a temperature of 65 °C and sheared at angular frequencies in the range between 0.1 and 200 Hz. The resulting values of the frequency-dependent modulus, $G(\omega) = G'(\omega) + iG''(\omega)$ were then measured and the time-dependent stress relaxation modulus, $G(t)$, was determined by Fourier transformation of the $G(\omega)$ data over the measured frequency range.

Results

Figure 1 shows optical micrographs of a PEO/PS bilayer (PS thickness $L = 143 \pm 5\,\mathrm{nm}$, PEO thickness $h = 533 \pm 6\,\mathrm{nm}$) supported on a Si substrate that were taken before and after heating to 70 °C. At room temperature and prior to heating, the surfaces of the PEO/PS bilayers are similar to those observed for the uncapped PEO films. After heating to 70 °C, the samples were observed to have a very different appearance. The periodic corrugations that were formed upon heating of the bilayers typically had wavelengths in the 1 to 40 μm range and could not be correlated with any of the structures that were observed prior to heating the samples. This morphology was also found to persist when the bilayer films were quenched to temperatures below the melting temperature of the PEO (63 °C). Some evidence of the crystallinity of the underlying PEO layers was observed on the samples following the quench, but the structures formed during recrystallisation of the PEO were similar to those observed prior to melting and were smaller (both laterally and vertically) than the lengthscales associated with the observed morphology.

Figure 2 shows AFM images of a spin cast PEO film ($h = 65 \pm 3\,\mathrm{nm}$, top panel) and the same PEO film after capping with a $44 \pm 4\,\mathrm{nm}$ thick PS film (middle panel). These images were taken at 25 °C over a scan area of $20\,\mu\mathrm{m} \times 20\,\mu\mathrm{m}$ and prior to heating the samples. This figure also shows an AFM image of the same sample, taken using a scan area of $20\,\mu\mathrm{m} \times 20\,\mu\mathrm{m}$, after heating to 70 °C for 10 seconds. Prior to imaging, this sample was rapidly quenched ($90\,^\circ\mathrm{C\,min^{-1}}$) to 50 °C, where the PEO layer was isothermally recrystallised. The PEO/PS bilayer film was then cooled to 25 °C and imaged (bottom panel). The insets in Figure 2 show the distribution of heights taken along a line on the samples before and after heating to 70 °C. These clearly show that the PS films faithfully follow the contours of the semicrystalline PEO surfaces and also that the surface structure of the bilayer changes significantly during the melting of the PEO layer. Both Figure 1 and Figure 2 show that the morphology that evolves when the bilayers are heated can be highly anisotropic. This is probably due to the presence of small anisotropic stresses that are introduced into the PS films during the water transfer technique used to prepare the bilayers. Samples that were produced in such a way as to minimise these additional stresses were shown to display more isotropic wrinkling morphologies. During prolonged annealing at 70 °C (~ 5 minutes), an increase/coarsening of the lateral wrinkling lengthscales was observed in both the anisotropic and isotropic samples. This coarsening is believed to occur as a result of the relaxation of residual bending stresses in the PS films. Although the system initially selects a characteristic lengthscale, the surface corrugations and hence the residual bending stresses in the PS can be removed by flow of material in the molten PEO underlayer. As a result of this, the lateral lengthscale was observed to increase while the amplitude of the undulation decreased. This continued until all the stresses in the films had been relaxed and the equilibrium state of the system occurred when the flat unstressed PS film rested on top of the molten PEO layer. At this point the observed morphology disappeared. These effects were observed for all the bilayers studied, but occurred more rapidly in bilayers that had thick PEO underlayers ($h = 533\,\mathrm{nm}$).

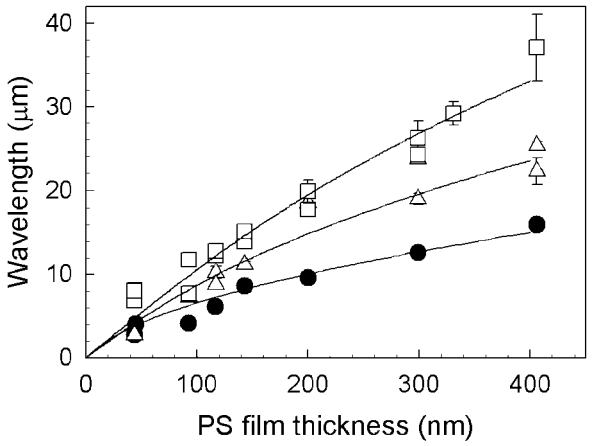

Fig. 3. Characteristic wavelength of the wrinkling morphology as a function of the PS capping layer thickness (L) . Data are shown for bilayer samples where the thickness (h) of the underlying PEO film was 65 nm (•), 211 nm (△) and 533 nm (□), respectively. The solid lines in this figure represent values of the fastest growing wavelength that were calculated from simulations of the amplitude growth rate, $s(q)$, that were determined using equation (6). In the simulations, values of $E = 3.4\,\mathrm{GPa}$ and $\nu = 0.325$ were used for the Young's modulus and Poisson ratio of the PS film and values of $\epsilon = 0.5 \times 10^{-3}$ and $G_o = 2.5\,\mathrm{kPa}$ were used for the strain in the PS films and the early-time value of the stress relaxation modulus, respectively (see text).

The plot in Figure 3 shows data for the wavelength of the observed morphology, that were determined from optical micrographs of the samples taken within ~ 1 second of the PEO layer melting. The dependence of the inital wrinkling wavelength on the PS capping layer thickness, L, is shown for three different values of the PEO thickness (h). This figure shows that it is possible to tune the wavelength of the observed morphology by varying the

thickness of the PEO under layer and/or the PS capping layer thickness.

Measurements of the total area of the PEO/PS bilayers taken from the AFM images collected before and after heating to 70 °C showed that the total surface area of the samples remains unchanged within error during the formation of the wrinkling morphology. This behaviour is consistent with a buckling phenomenon that is observed when a thin plate or film is compressed laterally at its sides [6,7]. The idea being that compressing the film or plate causes it to buckle with some characteristic wavelength that can be determined by balancing the membrane stresses in the film/plate prior to buckling and the bending stresses in the plate after buckling.

Discussion

Figure 4 shows a schematic diagram of the proposed mechanism for the formation of the observed wrinkling morphology in the PEO/PS bilayers studied here. Initially, the PS capping layer follows the contours of the rough PEO surface (a). When the PEO films are melted the roughness due to the crystallinity in the material disappears and surface tension flattens the surface of the molten PEO. Given that the PS film does not delaminate from the molten PEO film, the melting of this layer is expected to reduce the area of the PS capping layer, leaving it in a state of compressive strain (b). This strain arises because the PS film goes from having an area close to that of the total area of the uncapped PEO film to having an area that is essentially equal to that of the smooth Si substrate. Thermally driven fluctuations at the PEO/PS interface are then expected to cause deflections of the PS capping layer out of the plane of the bilayer samples and the PS film will start to buckle. The stresses introduced into the PS capping layers by changes in PEO/PS interfacial area are then expected to drive the buckling instability (c).

The buckling of the PS capping layer must also be accompanied by deformations of the underlying PEO and the viscoelastic response of this layer is expected to contribute to the selection of the dominant wavelength in this system. It is also important to note that this model assumes that the PS films do not initially contain any stresses such as those that might be introduced by elastic deformations of the films caused by surface forces. This is because the melting of the PEO would simply act to relax these elastic deformations and the morphology would not be expected to form. These factors are discussed in more detail below. In trying to describe what drives the buckling process, we must consider the balance of forces acting on the PS film and the flow in the viscoelastic PEO layer. This will allow us to derive an expression to determine the wrinkling wave vectors that have the fastest growing amplitudes. In all that follows we will restrict the analysis to a system that exhibits wrinkling in only one dimension. We will also assume that the vertical deflection, $w(x,t)$, is small in comparison to the thickness of the PS film at early times.

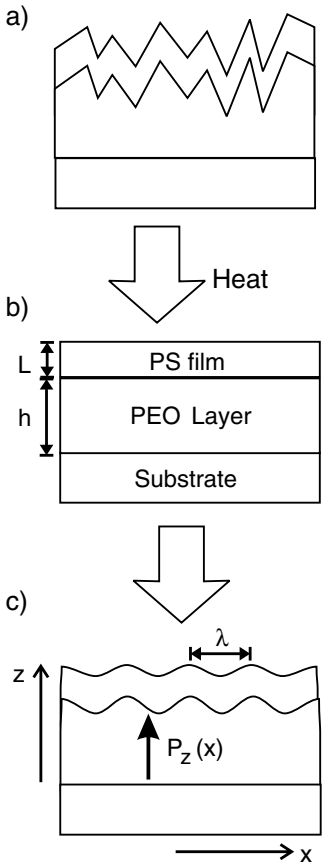

Fig. 4. Diagram showing the proposed mechanism for the formation of the observed wrinkling morphology in a thin-film bilayer comprising a PEO layer of thickness h, supported on a silicon substrate, with a PS capping layer of thickness L. Initially, the PS films faithfully follow the contours of the semicrystalline PEO surface (a). When the bilayer is heated above the melting temperature of PEO, the PEO/PS interfacial tension pulls the bilayer interface flat and leaves the PS capping layer in a state of compressive stress (b). These stresses are relaxed by bending the film and the system wrinkles with a characteristic wavelength λ (c). The wrinkled PS capping layer exerts a spatially dependent pressure on the the underlying PEO layer ($P_z(x)$) that determines the flow in this layer.

Linear stability analysis of bilayer wrinkling

We begin by using a simple analysis based upon the forces acting upon an elastic plate in a state of in-plane compressive stress. The pressure, $P_z(x)$, that is required to hold the film in a given shape at a point x, along the film (see Fig. 4) can be written in the form [15]

$$P_z(x) = \frac{EL^3}{12(1-\nu^2)}\frac{\mathrm{d}^4 h}{\mathrm{d}x^4} + E\epsilon L\frac{\mathrm{d}^2 h}{\mathrm{d}x^2} - \sigma_{zz}, \qquad (1)$$

where $h(x,t) = h_o + w(x,t)$ is the total thickness of the bilayer at a point, x, and time, t, h_o is the average thickness of the molten PEO layer and ϵ is the linear strain introduced into the PS film due to changes in the PEO/PS interfacial area. The quantities E, L and ν are the Young's

modulus, thickness and Poisson's ratio of the PS film, respectively.

The first term in equation (1) is the vertical component of the pressure exerted by the wrinkled film due to local bending. The second term occurs as a result of the membrane forces within the thin PS film that contain an out-of-plane component when the thin PS film starts to buckle. The third term, σ_{zz}, is the normal pressure exerted on the PS capping layer due to the viscoelastic response of the molten PEO film that occurs during its deformation by the wrinkling PS film.

In deriving equation (1) we have neglected to include a term describing the effects of dispersion forces between the capping layer and the substrate. Our justification for neglecting these forces comes from our observation that bilayers produced when the PEO is in the molten state do not wrinkle. Under these conditions dispersion forces would also be expected to be present and we would therefore expect to observe wrinkles if these forces were significant. However, we note that for thinner PEO underlayers ($\sim$ 10 nm thick) a term describing the dispersion forces between the capping layer and the susbstrate should be included in equation (1) as these forces would be much larger in magnitude and would contribute to the final wrinkling morphology.

A consideration of the Poiseuille flow, J, in the PEO layer gives that

$$J = -\frac{h^3}{3\eta}\frac{\mathrm{d}P}{\mathrm{d}x}\,, \tag{2}$$

where η is the viscosity of the PEO. The assumption of incompressibility in the PEO layer results in the conservation of volume and the condition that

$$\frac{\mathrm{d}h}{\mathrm{d}t} = -\frac{\mathrm{d}J}{\mathrm{d}x}. \tag{3}$$

Matching the displacements at the PEO/PS interface and combining equations (1), (2) and (3) results in an expression that describes the time-dependent evolution of local variations in the height of the surface of the bilayer, such that

$$\frac{\mathrm{d}h}{\mathrm{d}t} = \frac{h^3}{3\eta}\left(\frac{EL^3}{12(1-\nu^2)}\frac{\mathrm{d}^6h}{\mathrm{d}x^6} + E\epsilon L\frac{\mathrm{d}^4h}{\mathrm{d}x^4} - \frac{\mathrm{d}^2\sigma_{zz}}{\mathrm{d}x^2}\right). \tag{4}$$

This expression is similar to that derived by Yoo *et al.* [16,17] for the so-called *spinodal wrinkling* of polymer/metal bilayers. This term was chosen because the wrinkling transition that occurs in polymer/polymer and polymer/metal bilayers has some features that are similar to those observed in processes such as spinodal decomposition and spinodal dewetting. The main similarities are that the processes are driven by thermal fluctuations and that each system selects a characteristic wavelength as a result of competing physical processes. However, unlike processes such as spinodal decomposition and spinodal dewetting there is no underlying thermodynamic transition responsible for the lengthscale selection in the case of spinodal wrinkling. In the absence of in-plane strains introduced by changing interfacial roughness (or by diferential thermal expansion coefficients) the wrinkling transition does not occur, whereas a homogeneous blend of two polymers can phase-separate via spinodal decomposition and a thin fluid film of intitially uniform thickness can undergo spinodal dewetting.

In the study by Yoo *et al.*, the difference in the thermal expansion coefficients of the PS and aluminium layers studied was shown to result in a compressive stress being exerted on the metal films when the temperature of the samples was changed. These authors derived an approximate form for the spatial dependence of the normal pressure exerted by the viscoelastic PS layer on the metal film [17] that was based upon a correlation method. This correlation method was constructed using a combination of the long- and short-wavelength limit asymptotic values of the free energy of deformation, F, of a film subjected to a sinusoidal surface perturbation. These authors showed that this simplified form for the free energy accurately fits the analytical solutions derived previously by Fredrickson and coworkers [18] and Xi and Milner [19].

The analytical solutions for the normal pressure produced in the viscoelastic underlayer were determined by assuming zero displacement boundary conditions at the substrate interface, periodic lateral boundary conditions in the stress in the bilayers and that no tangential stresses were present at the polymer/metal interface [18]. Yoo and coworkers then used their approximate form for the free energy of deformation to derive an equation for the normal pressure exerted by the viscoelastic polymer layer on the metal film such that $\sigma_{zz} = \frac{\mathrm{d}F}{\mathrm{d}h}$. This gave the result that

$$\sigma_{zz} = A(t)G_o\cos(qx)\left(\frac{q}{2} + \frac{3}{4q^2h^3} + \frac{1.87}{2q^{1.4}h^{2.4}}\right), \tag{5}$$

where $A(t)$ is the time-dependent amplitude of the sinusoidal perturbation at the surface and G_o is the value of the early-time stress relaxation modulus of the viscoelastic polymer underlayer.

In the present study, we assume that the molten PEO layer exerts a similar pressure on the wrinkling PS films at early times (*i.e.* immediately after melting) and proceed as per the analysis of Yoo *et al.* We assume that the average thickness of the PEO layer, h_o is large in comparison to the early time deflections of the PS film. This allows us to linearise equation (4) and assume a solution of the form $h(x) = h_o + A(t)\cos qx$. Inserting these results into the expression obtained by combining equations (4) and (5), gives an expression for the time evolution of the amplitude of a surface fluctuation of wave vector q, that has the form $\frac{\mathrm{d}A}{\mathrm{d}t} = s(q)A(t)$, where $s(q)$ is the wave-vector–dependent growth rate of the amplitude fluctuations. Solving the resulting equation then gives an expression for $s(q)$ of the form

$$s(q) = \frac{h_o^3}{3\eta}\left(-\frac{EL^3}{12(1-\nu^2)}q^6 + E\epsilon Lq^4 + G_o\left(\frac{q^3}{2} + \frac{3}{4h_o^3} + \frac{0.905q^{0.6}}{h_o^{2.4}}\right)\right). \tag{6}$$

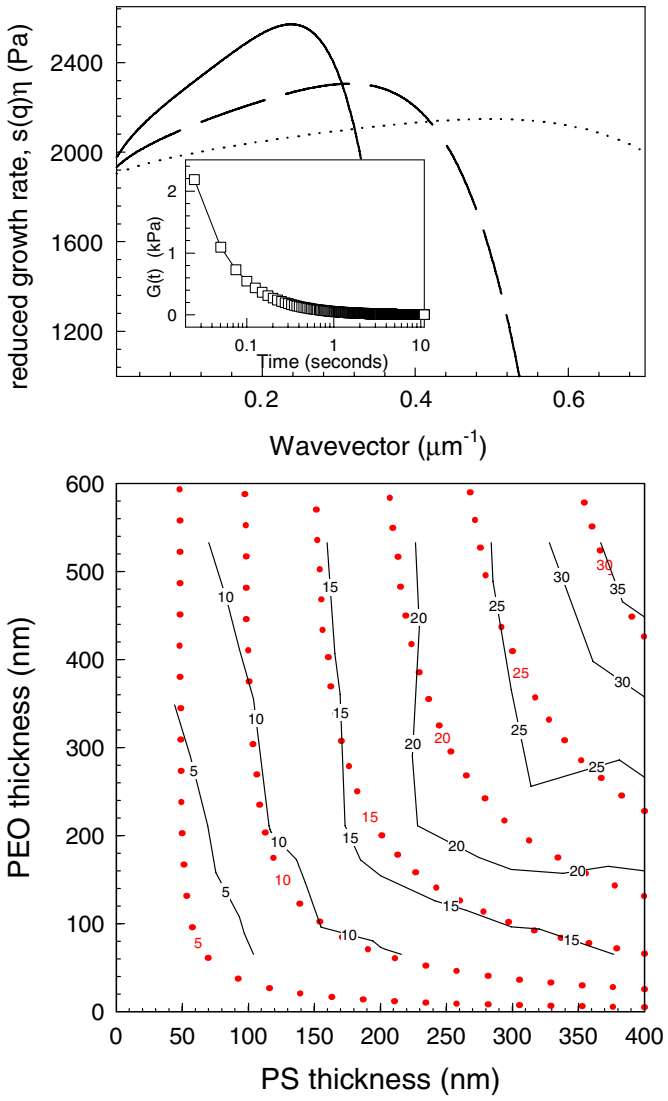

Fig. 5. Plot of the results of simulations of the normalised amplitude growth rate, $s(q)$, for sinusoidal surface fluctuations of the wave vector, q (as determined from Eq. (6)). The top panel shows simulation results for model PEO/PS bilayers with a PS layer thickness of $L = 300\,\text{nm}$ and PEO layer thicknesses of $h = 65\,\text{nm}$ (dotted line), $h = 211\,\text{nm}$ (dashed line) and $h = 533\,\text{nm}$ (solid line), respectively. Values of $E = 3.4\,\text{GPa}$ and $\nu = 0.325$ were used for the Young's modulus and Poisson ratio of the PS film and values of $\epsilon = 0.5 \times 10^{-3}$ and $G_o = 2.5\,\text{kPa}$ were used for the strain in the PS films and the early-time value of the stress relaxation modulus (see text). The inset (top panel) shows the time dependence of the stress relaxation modulus for a 10k M_w PEO that was determined by Fourier transformation of the complex frequency-dependent modulus $G(\omega) = G'(\omega) + iG''(\omega)$. The bottom panel shows a contour plot of the the inital wavelength as a function of both the PS and PEO film thicknesses (h and L, respectively). The dotted lines represent contours of constant wavelength (measured in microns) that were determined from the results of simulations based on equation (6). The solid lines are similar contours that were determined from the experimental data shown in Figure 3.

For values of $s(q) < 0$, the amplitude of fluctuations will be strongly damped, while for values of $s(q) > 0$ fluctuations of a given wave vector are expected to be amplified. Figure 5 shows a plot of the reduced growth rate $s(q)\eta$ as a function of the wave vector, q, for different values of the the PEO and PS film thicknesses, $h(= h_o)$ and L, respectively. These plots clearly indicate that equation (6) predicts the existence of a fastest growing wavelength in the model system proposed. The wave vector, q_{max} with the fastest growing amplitude is therefore expected to dominate the observed wrinkling morphology at early times and is given by the condition that $\frac{\mathrm{d}s}{\mathrm{d}q} = 0$. The faster growth rates that are predicted for larger values of h, also support the observation of more rapid coarsening of the measured wavelengths in bilayers that were produced using thick ($h = 533\,\text{nm}$) PEO films.

Comparison between theory and results

Plots of the reduced growth rate, $s(q)\eta$, as a function of q, similar to those shown in the top panel of Figure 5, were used to determine q_{max} for different combinations of the PS and PEO layer thicknesses, h and L. Values of the dominant wavelength in the system, were then calculated using the expression $\lambda = 2\pi/q_{max}$. The values that were obtained from these simulations are plotted in Figure 3 as the solid lines. In all cases values of $E = 3.4\,\text{GPa}$ and $\nu = 0.325$ were used for the Young's modulus and Poisson ratio of glassy PS, respectively [12]. Values of the linear strain, $\epsilon = \epsilon_{lin}$, in the PS films were then determined from the AFM measurements of the PEO/PS bilayer surfaces. As described above, the surface area of the bilayers was used to obtain an estimate for the linear strain in the PS of $\epsilon_{lin} = (0.50 \pm 0.05) \times 10^{-3}$.

The use of this value for the strain, assumes that the PS films are in an unstressed state prior to the melting of the PEO. There are two possible ways in which this could occur. The first possibility is that during the formation of the bilayers, the surface forces that pull the two films into contact could cause large local extensions in the PS films as they conform to the PEO surface. If these deformations were large enough to cause the onset of yield in the PS films, then the plastic deformation of the PS would allow the films to relax the stresses introduced by the production of the bilayer. In the absence of yield processes, the deformations in the films introduced during bilayer preparation would result in purely elastic deformations of the PS capping layers. The melting of the PEO layer would then simply act to relax these elastic deformations and the morphology would not be observed. A simple calculation of the typical stress, $\sigma_{prep}(= E\epsilon_{lin})$, that would be caused by the preparation of the bilayers, gives a value of $\sigma_{prep} = 1.7\,\text{MPa}$. This is much lower than the measured stress value of $\sim 30\,\text{MPa}$ ($\epsilon_{lin} \sim 0.01$) obtained for the onset of non-linear mechanical processes in PS [20]. This would seem to indicate that yield does not occur in the PS capping layers. An alternative explanation for the presence of little or no stress in the capping layers could be that there was some slack in the freely

standing PS films that were used to produce them. Although these freely standing films were annealed to remove short-wavelength wrinkles and defects, the removal of slack in the films would be expected to occur on longer time scales because of the need to transport material over larger distances. This would mean that although annealing the PS films above a hot plate could be used to relieve local spin coating stresses and to remove local defects, the films would not be pulled into tension. As a result of this, when the PS films were used to produce the bilayer samples, the deformations caused by the surfaces forces pulling the two films into contact could be compensated for by the slack in the PS films. This would result in the PS capping layers being unstressed following bilayer formation. However, although both of these effects provide possible explanations for why we might expect the PS to be stress free, they are extremely difficult to quantify in the context of the present experiments.

The bottom panel in Figure 5 shows a contour plot of the PS and PEO film thickness (h and L, respectively) dependence of the fastest growing wavelength. In this plot, the dotted lines represent contours of constant wavelength (measured in microns) that were calculated using equation (6). The solid lines represent similar contours that were determined from the experimental data. This plot in conjunction with Figure 3 shows that there is good agreement between the predictions of the proposed theory and experiment in terms of describing both the h- and L-dependence of the fastest growing wavelength in the system. In addition, the contour plot shown in Figure 5 allows us to find combinations of h and L that will enable us to produce any desired wavelength for the wrinkling morphology studied within the range of wavelengths reported.

A comparison of the experimental values of the dominant wavelength, λ, with those obtained from the results of the simulations shown in Figures 3 and 5, illustrates that they are in extremely good agreement and indicates that the suggested mechanism for the formation of the wrinkling morphology is likely to be the correct one. In all cases a value of the early-time stress relaxation modulus of the PEO of $G_o = 2.5 \pm 0.1$ kPa was found to best fit the experimental data. The value of G_o determined from the results of our experiments is significantly smaller than the values reported by Yoo and coworkers [17] for the PS/metal bilayer system (30–500 kPa). However, this is to be expected based upon the differences in the physical properties of the materials and the different temperatures used in the separate studies. To determine whether the value of G_o used in the simulations accurately describes the material properties of the PEO underlayer at early times and at the temperatures studied in the present work, measurements of the frequency-dependent modulus ($G(\omega) = G'(\omega) + iG''(\omega)$) of a 10k M_w PEO were taken at a temperature of 65 °C (as described in the experimental section). The value of $G(\omega)$ was then Fourier transformed to give the time-dependent stress relaxation modulus, $G(t)$. The inset in Figure 5 shows a plot of $G(t)$ as a function of time and shows that the early-time values of $G(t)$ are in the 2–3 kPa range. This is in good agreement with the value of G_o determined from the simulations of the wrinkling and again confirms the validity of the theoretical approach described above.

A consideration of equation (6) shows that the term describing the viscoelastic response of the PEO layer is needed to obtain the agreement between the theory and the experimental data and to predict the PEO thickness dependence of the fastest growing wavelength shown in Figure 3. In the absence of this term, equation (6) reduces to a form where the characteristic wavelength has the following functional dependence $\lambda = \pi L(\frac{1}{2\epsilon(1-\nu^2)})^{\frac{1}{2}}$. This clearly predicts that the wavelength obtained should depend only upon the thickness of the PS capping layer (L) and should have no dependence upon the thickness of the PEO layer. As described above, the fastest growing wavelength in the system is dependent upon both the thickness of the PEO layer and the PS capping layer. In addition, the linear dependence of the wavelength on L that is predicted by this simplified equation does not fit the apparent curvature that is observed at large values of L in the data for the bilayer film thicknesses studied (see Fig. 3). One possible way to try to model the h-dependence of the observed morphology would be to include a thickness-dependent strain in our calculations. A similar h-dependent strain is also required to obtain agreement between the data and existing theoretical models that have been developed to describe the wrinkling of elastic films on viscous [9,10] and viscoelastic substrates [11]. However, the observation that all the PEO/PS bilayers studied had approximately the same surface area prior to heating rules out the possibilty of a PEO thickness-dependent strain in this system.

Conclusions

We have shown that thin-film bilayers of poly(ethylene oxide) (PEO) and polystyrene (PS) undergo a wrinkling instability when the bilayers are heated above the melting temperature of the PEO. The wrinkling instability was shown to be driven by changes in the area of the PEO/PS interface that occur when the semicrystalline PEO layer melts. The change in the area of this interface causes the glassy PS capping layer to reduce its area and introduces a compressive strain into this layer. The resulting stresses drive the wrinkling instability and the amplitude of fluctuations with a characteristic lengthscale are shown to grow faster than for all other wavelengths. This results in a series of periodic corrugations at the surface of the bilayers with a well-defined wavelength. A simple theory based upon a linear stability analysis showed that the characteristic wrinkling wavelength is determined by a balance of the in-plane stresses in the PS films, the bending stresses in the buckled state and the viscoelastic properties of the PEO underlayer. Atomic force microscopy measurements of the surface areas of PEO films and PEO/PS bilayers before and after heating showed that the strains introduced during the melting of the PEO/PS bilayers are sufficient to drive the wrinkling instability. The simple theory showed

that the only parameters that are required to predict the characteristic wavelength in the system are the strain in the PS film after melting of the PEO layer, the thickness of the PS films and the bulk mechanical properties of the PS and PEO at the temperatures studied.

We would like to thank the Engineering and Physical Sciences Research Council (EPSRC), UK and the Natural Sciences and Engineering Research Council (NSERC) of Canada for funding this work. JSS also gratefully acknowledges the Nuffield Foundation for a New Lecturers Award and the PATTERNS Marie Curie Research Training Network (MRTN-CT-2004-005728, EU Framework Programme 6) for providing funding. JAF wishes to acknowledge insightful discussions with Z. Suo.

References

1. L. Rockford, S.G.J. Mochrie, T.P. Russell, Macromolecules **34**, 1487 (2001).
2. A.M. Higgins, R.A.L. Jones, Nature **404**, 476 (2000).
3. K. Dalnoki-Veress, B.G. Nickel, J.R. Dutcher, Phys. Rev. Lett. **82**, 1486 (1999).
4. E. Schäffer, T. Thurn-Albrecht, T.P. Russell, U. Steiner, Nature **403**, 874 (2000).
5. N. Bowden, S. Brittain, A.G. Evans, J.W. Hutchinson, G. Whitesides, Nature **393**, 146 (1998).
6. H.G. Allen, *Analysis and Design of Structural Sandwich Panels* (Pergamon Press, 1969).
7. J.S. Sharp, R.A.L. Jones, Phys. Rev. E **66**, 011801 (2002).
8. J.S. Sharp, R.A.L. Jones, Adv. Mater. **14**, 799 (2002).
9. R. Huang, Z. Suo, Int. J. Solids Struct. **39**, 1791 (2002).
10. N. Sridhar, D.J. Srolovitz, Z. Suo, Appl. Phys. Lett. **78**, 2482 (2001).
11. R. Huang, J. Mech. Phys. Solids **53**, 63 (2005).
12. J. Brandrup, E.H. Immergut (Editors), *Polymer Handbook*, 4th edition (Wiley, 1989).
13. R.M.A. Azzam, N.M. Bashara, *Ellipsometry and Polarized Light* (North Holland, Amsterdam, 1987).
14. J.A. Forrest, K. Dalnoki-Veress, J.R. Dutcher, Phys. Rev. E **56**, 5705 (1997).
15. L.G. Jaeger, *Elementary Theory of Elastic Plates* (Pergamon Press, 1964).
16. P.J. Yoo, H.H. Lee, Phys. Rev. Lett. **91**, 154502 (2003).
17. P.J. Yoo, K.Y. Suh, H. Kang, H.H. Lee, Phys. Rev. Lett. **93**, 034301 (2004).
18. G.H. Fredrickson, A. Ajdari, L. Leibler, J. Carton, Macromolecules **25**, 2882 (1992).
19. H. Xi, S.T. Milner, Macromolecules **29**, 4772 (1996).
20. G. Strobl, *The Physics of Polymers*, 2nd edition (Springer, Berlin-Heidelberg, 1997) p. 351.